Journal of Materials Chemistry A

ROYAL SOCIETY OF CHEMISTRY

PAPER

View Article Online
View Journal | View Issue

Cite this: *J. Mater. Chem. A*, 2020, **8**, 3613

Engineering microporous ethane-trapping metal–organic frameworks for boosting ethane/ethylene separation†

Jiyan Pei,[a] Jia-Xin Wang,[a] Kai Shao,[a] Yu Yang,[a] Yuanjing Cui,[a] Hui Wu,[b] Wei Zhou,*[b] Bin Li*[a] and Guodong Qian*[a]

Received 19th November 2019
Accepted 13th January 2020

DOI: 10.1039/c9ta12671f

rsc.li/materials-a

Realization of ethane-trapping materials for separating ethane (C_2H_6) from ethylene (C_2H_4) by adsorption, to potentially replace the energy-intensive cryogenic distillation technology, is of prime importance in the petrochemical industry. It is still very challenging to target C_2H_6-selective adsorbents with both high C_2H_6 capture capacity and gas selectivity. Herein, we report that a crystal engineering or reticular chemistry strategy enables the control of pore size and functionality in a family of isomorphic metal–organic frameworks (MOFs) for boosting the C_2H_6 uptake and selectivity simultaneously. By altering the carboxylic acid linker in Ni(bdc)(ted)$_{0.5}$, we developed two novel isoreticular MOFs, Ni(ndc)(ted)$_{0.5}$ and Ni(adc)(ted)$_{0.5}$ (termed ZJU-120 and ZJU-121, respectively), in which the pore sizes and nonpolar aromatic rings can be finely engineered. We discover that activated ZJU-120a with the optimized pore size (4.4 Å) and aromatic rings exhibits both a very high C_2H_6 uptake (96 $cm^3\ g^{-1}$ at 0.5 bar and 296 K) and C_2H_6/C_2H_4 selectivity (2.74), outperforming most of the C_2H_6-selective MOFs reported. Computational studies indicate that the suitable pore size and more nonpolar aromatic rings on the pore surfaces of ZJU-120a mainly contribute to its exceptional C_2H_6 uptake and selectivity. The breakthrough experiments demonstrate that ZJU-120a can efficiently separate C_2H_6 from 50/50 and 10/90C_2H_6/C_2H_4 mixtures under ambient conditions.

Introduction

Ethylene (C_2H_4) is a key raw material for the production of many chemicals and polymers, with a global production capacity exceeding 170 million tons in 2017. It is mostly produced by the steam cracking of ethane and liquefied petroleum gas and inevitably contains some other gaseous impurities (mostly C_2H_6).[1,2] The C_2H_6 impurity must be removed to produce polymer-grade (≥99.95% pure) C_2H_4 as the starting feedstock for polymer production.[3] Currently, this separation is mainly dominated by cryogenic distillation, which requires a repeated distillation–compression cycling of the mixture under high pressures and low temperatures (typically at 5–28 bar and 180–258 K using over 100 trays).[4,5] Obviously, this well-established industrial separation technology represents one of the most energy-intensive processes in the chemical industry. The total energy used for ethylene and propylene separations has been recently reported to account for more than 0.3% of the global energy consumption. Alternative separation techniques aiming to reduce the economic and energy costs are highly desirable and become of prime importance in the petrochemical industry.[6,7]

Adsorption separation based on porous materials is a promising technology that has the potential to replace the traditional cryogenic distillation and thus to obtain energy-efficient separation. A large number of porous materials, such as γ-Al_2O_3, zeolites, and metal–organic frameworks (MOFs), have been developed as adsorbents for C_2H_4/C_2H_6 separation.[8,9] Generally, these porous materials adsorb more amounts of C_2H_4 than that of C_2H_6, since the incorporated metal sites/clusters on the pore surfaces have stronger interactions with unsaturated C_2H_4 molecules through π-complexation.[10,11] Although some of these C_2H_4-selective adsorbents exhibit exceptional performance in C_2H_4/C_2H_6 separation, the pure C_2H_4 product, as the preferentially adsorbed gas, still requires an additional desorption step to be yielded under high temperature or vacuum conditions. To achieve polymer-grade purity, multiple adsorption–desorption purification cycles are necessary to be performed.

In this context, realization of C_2H_6-selective adsorbents is more desirable for this separation because high-purity C_2H_4 can be directly yielded during the adsorption step with significant

[a]State Key Laboratory of Silicon Materials, Cyrus Tang Center for Sensor Materials and Applications, Department of Materials Science & Engineering, Zhejiang University, Hangzhou 310027, China. E-mail: bin.li@zju.edu.cn; gdqian@zju.edu.cn

[b]NIST Center for Neutron Research, National Institute of Standards and Technology, Gaithersburg, MD 20899-6102, USA. E-mail: wzhou@nist.gov

† Electronic supplementary information (ESI) available: PXRD, crystal data, and adsorption isotherms of ZJU-120. CCDC 1953742. For ESI and crystallographic data in CIF or other electronic format see DOI: 10.1039/c9ta12671f

energy saving. Considering that ethane has a higher polarizability than ethylene (44.7×10^{-25} *vs.* 42.52×10^{-25} cm^3), a C_2H_6-selective adsorbent is typically required to possess a porous structure enriched with nonpolar/inert surfaces (*e.g.*, featuring aromatic or aliphatic moieties), wherein dispersion and induction interactions can make major contributions.[5] However, inorganic secondary building units (SBUs) in MOFs are commonly detrimental to the formation of nonpolar/inert surfaces, making most of them exhibit preferred C_2H_4 adsorption over C_2H_6. To date, only a handful of such C_2H_6-selective MOFs have been realized; however, most of them suffer from either poor selectivity or low C_2H_6 uptake.[12–20] For example, some benchmark C_2H_6-selective MOFs with specific C_2H_6-affinity sites can discriminate between C_2H_6 and C_2H_4 with a record high selectivity (2.7–4.4), while their moderate pore volumes lead to a relatively low C_2H_6 uptake (1.7–3.0 mmol g^{-1}).[12–14] On the other hand, construction of nonpolar/inert pore surfaces within MOFs is another strategy to realize C_2H_6-selective adsorption. Nevertheless, the lack of strong binding sites to recognize C_2H_6 molecules makes these materials suffer from poor selectivity (1.3–2.0), thus delimiting the separation performance toward C_2H_6/C_2H_4 mixtures.[15–20] Evidently, it remains a grand challenge to achieve both high C_2H_6 uptake capacity and C_2H_6/C_2H_4 selectivity in a single MOF material; however, both of them are two most important criteria that are directly related to C_2H_4 productivity and purity.

MOF chemistry has enabled us to precisely control and design structures, pore sizes, and functionalities at the molecular level to obtain excellent separation performance in a number of gas separation tasks.[21–25] We speculated that if we precisely optimize the pore size and functionality in C_2H_6-selective MOFs, the resulting materials have the potential to possess both high adsorption selectivity and uptake capacity for C_2H_6/C_2H_4 separation. With this in mind, we herein used a crystal engineering strategy to finely tailor the pore size and functionality in a family of isomorphic MOFs. We chose $Ni(bdc)(ted)_{0.5}$(bdc = 1,4-benzenedicarboxylic acid; ted = 1,4-diazabicyclo[2.2.2]octane) as the fundamental framework backbone because of its easily adjustable number of aromatic rings in the bdc linkers and its reversed C_2H_6/C_2H_4 adsorption with a high C_2H_6 uptake (5.13 mmol g^{-1}) but poor selectivity (1.8).[15] The use of 1,4-naphthalenedicarboxylic acid (H_2ndc) and 9,10-anthracenedicarboxylic acid (H_2adc) instead of H_2bdc afforded two novel MOFs, $Ni(ndc)(ted)_{0.5}$ (ZJU-120) and $Ni(adc)(ted)_{0.5}$ (ZJU-121). Compared with $Ni(bdc)(ted)_{0.5}$ (6.4 Å), ZJU-120 and ZJU-121 show a notably contracted pore size of 4.4 Å and 3.7 Å, respectively, along with more nonpolar aromatic rings on the pore surfaces. Gas sorption studies revealed that all of these activated MOFs show the preferential adsorption of C_2H_6 over C_2H_4. Amongst these MOFs, activated ZJU-120a with a medium pore size and nonpolar aromatic rings exhibits both a high C_2H_6 uptake capacity (96 cm^3 g^{-1} at 0.5 bar and 296 K) and C_2H_6/C_2H_4 selectivity (2.74 *vs.* 1.8 and 1.51 in $Ni(bdc)(ted)_{0.5}$ and ZJU-121a), both of which outperform most of the C_2H_6-selective MOFs reported. The exceptional separation performance of ZJU-120a was further confirmed by breakthrough experiments on both 50/50 and 10/90 C_2H_6/C_2H_4 mixtures.

Results and discussion

The reaction of nickel(II) chloride hexahydrate, H_2ndc and ted in *N*,*N*-dimethylmethanamide (DMF) solution at 393 K for 2 days afforded a green crystal sample of $Ni(ndc)(ted)_{0.5}$ (ZJU-120). Single crystal X-ray diffraction revealed that ZJU-120 has an isoreticular structure to $Ni(bdc)(ted)_{0.5}$, with a tetragonal $P4/mmm$ space group (Table S1, ESI†). The dark yellow powder sample of $Ni(adc)(ted)_{0.5}$ (ZJU-121) was synthesized through the same step by using H_2adc to replace H_2ndc as a linker. Despite extensive attempts, we were not able to obtain single crystals of ZJU-121 large enough for single-crystal X-ray diffraction studies. Fortunately, powder X-ray diffraction (PXRD) patterns indicate that ZJU-121 has a structure similar to that of ZJU-120. Therefore, structural determination was conducted on ZJU-121 through powder diffractometry using a direct method that was often used in our previous studies.[26] We modelled its structure using the same framework connection as ZJU-120 and then optimized the orientation of anthracene rings. The simulated PXRD pattern of our structural model agrees excellently with the experimental data (Fig. 2a and S3, ESI†), strongly supporting its validity.

$Ni(bdc)(ted)_{0.5}$, ZJU-120 and ZJU-121 together form an interesting series of isoreticular MOFs. All three frameworks are composed of paddlewheel dinuclear $Ni_2(COO)_4$ secondary building units (SBUs) bridged by dicarboxylate ligands to form a two-dimensional (2D) square-grid. The neighboring 2D grids are pillared by the ted to construct a three-dimensionally extended framework. The use of different dicarboxylate linkers guided by the crystal engineering strategy enables fine-tuning of the pore size and chemistry in these frameworks. As shown in Fig. 1, $Ni(bdc)(ted)_{0.5}$ possesses square channels of pore dimensions of 6.4 Å. When using ndc instead of bdc as a linker, the resulting ZJU-120 exhibits a significantly contracted pore size of 4.4 Å, mainly attributed to the tilting of bulky naphthalene rings pointing into the pores. Furthermore, the incorporation of anthracene rings into the framework affords smaller pores of 3.7 Å in ZJU-121. Pore sizes in this series therefore range from 6.4 Å to 3.7 Å. In addition, the introduced naphthalene or anthracene rings in ZJU-120 or ZJU-121 can provide more C–H$\cdots\pi$ interactions with C_2H_6 molecules which are beneficial for the preferential binding of C_2H_6 over C_2H_4. Evidently, the fine-tuned pore sizes and nonpolar aromatic rings in this series of isomorphic MOFs offer us great potential to optimize the C_2H_6/C_2H_4 separation performance.

Prior to the gas sorption measurements, we first investigated the air and humidity stability of ZJU-120 and ZJU-121. As shown in Fig. S4 and S5 (ESI†), when the as-synthesized samples were exposed to air for more than one month, the frameworks of ZJU-120 and ZJU-121 still retain their structural integrity. During the exposure of ZJU-120 and ZJU-121 to a 60%-humidity environment, no loss of crystallinity and no phase change were observed, indicating their good stability against moisture. Various temperature PXRD patterns revealed that both frameworks exhibit an excellent thermal stability up to 300 °C without phase changes observed (Fig. S8 and S9, ESI†). Next, the

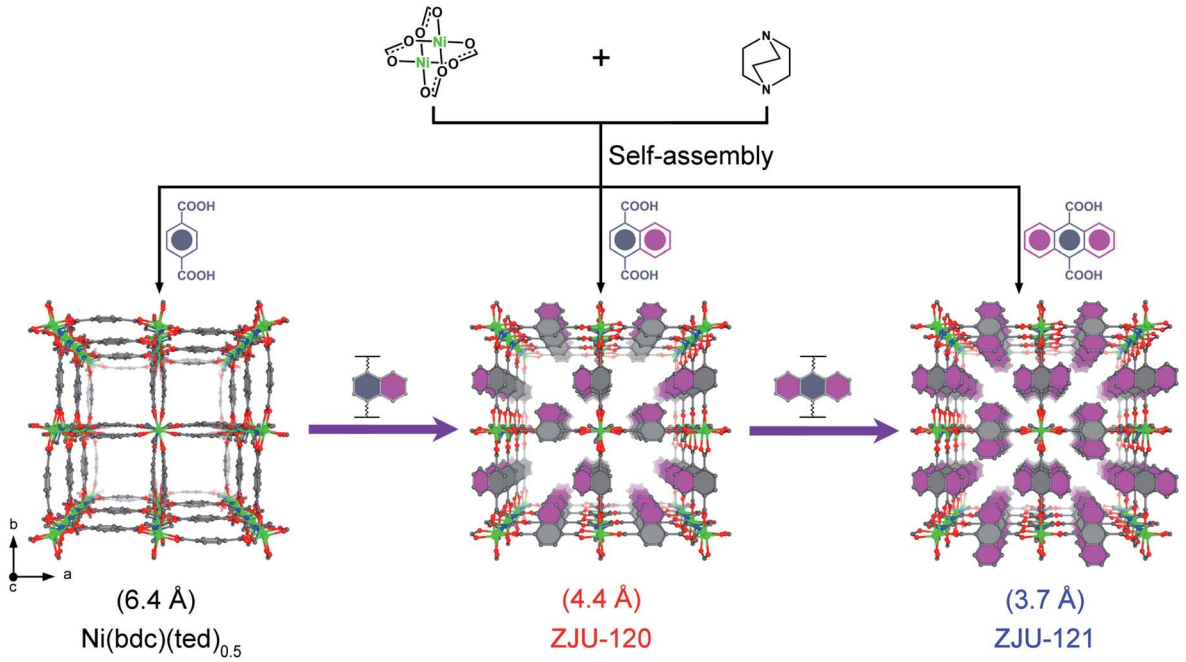

Fig. 1 Structure description of Ni(bdc)(ted)$_{0.5}$, ZJU-120 and ZJU-121, revealing the contracted pore size by introducing aromatic rings in the channels. Colour code: Ni (green), O (red), N (blue), and C (grey).

permanent porosity of activated ZJU-120a and ZJU-121a was confirmed by nitrogen (N_2) adsorption isotherms at 77 K. As shown in Fig. 2b, the saturated N_2 uptakes of ZJU-120a and ZJU-121a are 389 and 228 cm^3 g^{-1}, respectively, notably lower than that of Ni(bdc)(ted)$_{0.5}$ (626 cm^3 g^{-1}). The Brunauer–Emmett–Teller (BET) surface area of Ni(bdc)(ted)$_{0.5}$, ZJU-120a and ZJU-121a also gradually decreased from 2791, 1597 to 923 m^2 g^{-1} (Fig. S12–S14, ESI†), respectively, mainly attributed to the

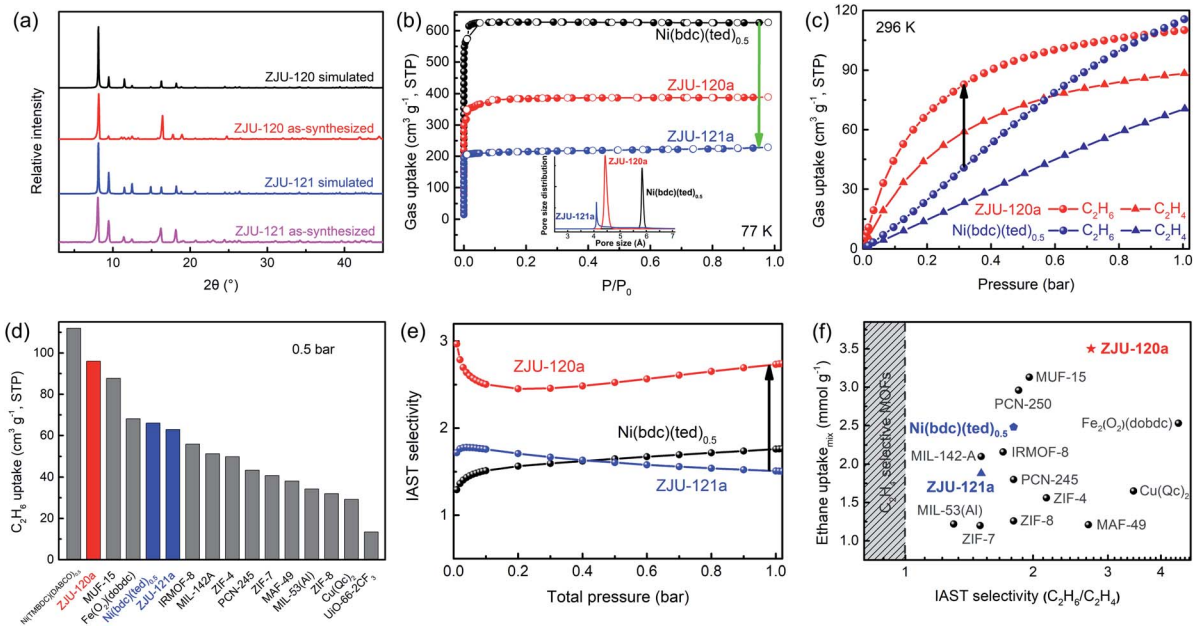

Fig. 2 (a) The simulated XRD patterns of the structure of ZJU-120 (black) and ZJU-121 (blue) compared with PXRD patterns of as-synthesized ZJU-120 (red) and ZJU-121 (purple). (b) Gas adsorption isotherms of Ni(bdc)(ted)$_{0.5}$, ZJU-120a and ZJU-121a for N_2 at 77 K. Filled/empty symbols represent adsorption/desorption. Inset shows pore size distribution for Ni(bdc)(ted)$_{0.5}$, ZJU-120a and ZJU-121a, based on the Horvath–Kawazoe model. (c) Gas adsorption isotherms of ZJU-120a and Ni(bdc)(ted)$_{0.5}$ for C_2H_6 and C_2H_4 at 296 K. (d) Comparison of the C_2H_6 capture capacity of ZJU-120a and other best-performing materials at 0.5 bar and room temperature. (e) Selectivity of Ni(bdc)(ted)$_{0.5}$, ZJU-120a and ZJU-121a predicted by the IAST method for a 50/50C_2H_6/C_2H_4 mixture at 296 K. (f) C_2H_6 uptake from an equimolar mixture of C_2H_6/C_2H_4 as a function of IAST selectivity for the best ethane-selective materials at 1 bar and room temperature.

incorporated naphthalene or anthracene rings in the pores. In addition, the pore sizes calculated using the Horvath–Kawazoe model show the same decrease trend, in the order of Ni(bdc)(ted)$_{0.5}$ (5.8 Å) > ZJU-120a (4.4 Å) > ZJU-120a (4.1 Å) (Fig. 2b), in good agreement with the results obtained from the crystal structure.

The fine-tuned pore size and chemistry in this series of MOFs encouraged us to record their single-component adsorption isotherms of C_2H_6 and C_2H_4 at 273 and 296 K up to 1 bar. Similar to Ni(bdc)(ted)$_{0.5}$, ZJU-120a exhibits an obviously preferential binding of C_2H_6 over C_2H_4, in which the C_2H_6 uptake (110 cm^3 g^{-1}) is much higher than that of C_2H_4 (88 cm^3 g^{-1}) at 1 bar and 296 K (Fig. 2c). This C_2H_6 uptake at 1 bar is comparable to that of Ni(bdc)(ted)$_{0.5}$ (115 cm^3 g^{-1}) thanks to their similar structures. However, ZJU-120a shows a steeper and higher C_2H_6 uptake at low pressure compared with Ni(bdc) (ted)$_{0.5}$, probably attributed to the contracted pore size and more aromatic rings in ZJU-120a that result in a stronger C_2H_6 binding affinity. This can be well confirmed by the experimental isosteric heat of adsorption (Q_{st}), wherein the initial Q_{st} value of ZJU-120a (27.6 kJ mol^{-1}) is much higher than that of Ni(bdc)(ted)$_{0.5}$ (21 kJ mol^{-1}) (Fig. S21 and S24, ESI†). Therefore, at a partial pressure of 0.5 bar for 50/50 gas mixtures, ZJU-120a exhibits a notably enhanced C_2H_6 uptake (96 cm^3 g^{-1}) *versus* Ni(bdc)(ted)$_{0.5}$ (66 cm^3 g^{-1}). In comparison to other top-performing C_2H_6-selective materials, we found that ZJU-120a reaches an extremely high C_2H_6 uptake at 0.5 bar (Fig. 2d), only lower than that of the recently reported Ni(TMBDC)(DABCO)$_{0.5}$ (112 cm^3 g^{-1})[16] but higher than those of benchmark Fe$_2$(O$_2$)(dobdc) (68 cm^3 g^{-1})[12] and MUF-15 (87 cm^3 g^{-1}),[17] indicating its ultrastrong C_2H_6 capture capacity. When anthracene rings were incorporated into ZJU-121a, the C_2H_6 adsorption isotherms become steeper than those of ZJU-120a, while the C_2H_6 uptake (60 cm^3 g^{-1}) at 0.5 bar is much lower than that of ZJU-120a due to its too small pore volume. In addition, ZJU-121a shows very close adsorption isotherms for C_2H_6 and C_2H_4, making it very difficult to discriminate between them. This is likely because the smaller pore size and more aromatic rings in ZJU-121a can improve both C_2H_4 and C_2H_6 binding strength significantly, as indicated by the very high and close Q_{st} values for C_2H_6 (47.1 kJ mol^{-1}) and C_2H_4 (43.0 kJ mol^{-1}) (Fig. S27, ESI†). Therefore, our results indicate that properly optimizing the pore size and nonpolar aromatic rings in C_2H_6-selective MOFs can efficiently enhance the C_2H_6 uptake capacity in the low-pressure region, thus potentially benefiting the separation performance.

The adsorption selectivity of ZJU-120a and ZJU-121a for 50/50 (v/v) C_2H_6/C_2H_4 mixtures was predicted by using ideal adsorbed solution theory (IAST), respectively. As shown in Fig. 2e, ZJU-120a exhibits a high selectivity of 2.74 for 50/50 (v/v) C_2H_6/C_2H_4 mixtures at 1 bar and 296 K, which is over 50% larger than that of Ni(bdc)(ted)$_{0.5}$ (1.8) and ZJU-121a (1.51). This value is also higher than that of most top-performing MOFs reported (Fig. 2f and Table S5†), and only lower than that of benchmark Fe$_2$(O$_2$)(dobdc) (4.4)[12] and Cu(Qc)$_2$ (3.4).[13] It is worth noting that high C_2H_6 uptake capacity is also very important for the separation of 50/50 mixtures. Due to the suitable pore size and binding affinity to C_2H_6 molecules, we found that ZJU-120a shows an extremely high C_2H_6 uptake (3.51 mmol g^{-1}) from an equimolar mixture of C_2H_6/C_2H_4 as a function of IAST selectivity. To our knowledge, this value is the highest among those of all the C_2H_6-selective MOFs reported so far (Fig. 2f), even exceeding that of the benchmark materials such as MUF-15 (3.13 mmol g^{-1}),[17] Fe$_2$(O$_2$)(dobdc) (2.53 mmol g^{-1}),[12] Cu(Qc)$_2$ (1.65 mmol g^{-1}),[13] and MAF-49 (1.21 mmol g^{-1})[14] (Table S5, ESI†). Taken together, unlike most of the previously reported C_2H_6-selective MOFs that commonly have either low C_2H_6 uptakes or poor selectivity (Fig. 2f), ZJU-120a here exhibits a rare combination of both very high C_2H_6/C_2H_4 selectivity and C_2H_6 adsorption capacity, making it among the best-performing porous material for this industrially important separation.

To further understand the origin of the enhanced C_2H_6 uptake and the improved C_2H_6/C_2H_4 selectivity of ZJU-120a at the molecular level, we performed theoretical computations using the first-principles dispersion-corrected density functional theory (DFT-D) method. Calculations were carried out on both ZJU-120a and Ni(bdc)(ted)$_{0.5}$, for comparison purposes. Optimal adsorption configurations of C_2H_6 and C_2H_4 were identified and are schematically shown in Fig. 3a–c and S30–S32 (ESI†). In ZJU-120a, the C_2H_6 molecule interacts with four aromatic rings originated from two opposite naphthalene rings to form six C–H$\cdots\pi$ interactions (H$\cdots\pi$ 2.935(1)–4.197(3) Å; C–H$\cdots\pi$ 3.410 (0)–4.308(0) Å) (Fig. 3a), which are comparable with the sum of the vdW radii of hydrogen/carbon (1.20/1.70 Å) and carbon (1.70 Å) atoms. In contrast, there are only four C–H$\cdots\pi$ interactions (H$\cdots\pi$ 3.154(4)–3.703(5) Å; C–H$\cdots\pi$ 3.773(8)–4.138(8) Å) formed by the C_2H_4 molecule with three aromatic rings (Fig. 3b). As a result, C_2H_6 interacts more strongly with the framework than C_2H_4, mainly because of its larger molecular size and more number of C–H$\cdots\pi$ interactions. This can be further confirmed by the higher calculated static binding energies of C_2H_6 (37.2 kJ mol^{-1}) than C_2H_4 (32.3 kJ mol^{-1}) in ZJU-120a. Due to the larger pore size of Ni(bdc)(ted)$_{0.5}$, the C_2H_6 and C_2H_4 molecules are located at the corners of the pores and interact with two aromatic rings from two adjacent bdc ligands (Fig. 3c and S30†). Four hydrogen atoms in the C_2H_6 molecule could generate C–H$\cdots\pi$ interactions with two aromatic rings in Ni(bdc)(ted)$_{0.5}$. Thus, its weaker C_2H_6 binding affinity compared with ZJU-120a can be attributed to the larger pore size and the reduced number of C–H$\cdots\pi$ interactions, as also supported by the lower static binding energy (27.9 kJ mol^{-1}). These calculation results are fully consistent with our experimental findings discussed earlier.

Finally, we performed breakthrough experiments in a packed column of activated ZJU-120a to evaluate its separation performance for both actual 50/50 and 10/90C_2H_6/C_2H_4 mixtures at room temperature. As shown in Fig. 3d and e, it was clear that ZJU-120a can effectively separate both C_2H_6/C_2H_4 mixtures, wherein C_2H_4 gas passed through the adsorption bed first to yield pure gas with an undetectable amount of C_2H_6 (the detection limit of the instrument is 0.01%), directly producing a desirable purity of over 99.95%. Conversely, C_2H_6 breakthrough occurred after a period of time since C_2H_6 can be more

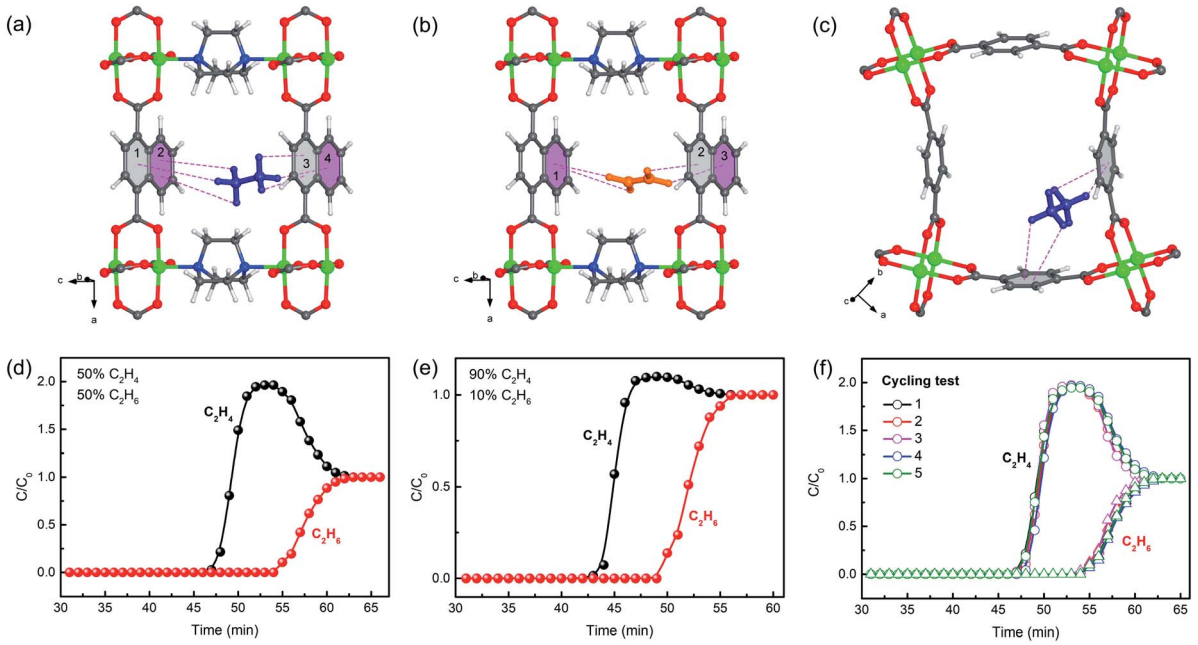

Fig. 3 Comparison of the optimal (a) C_2H_6 and (b) C_2H_4 adsorption sites in ZJU-120a and (c) the C_2H_6 adsorption site in Ni(bdc)(ted)$_{0.5}$ obtained from DFT-D calculations. Colour code: Ni (green), O (red), N (blue), C (grey), and H (white). Experimental column breakthrough curves of (d) a 50/50C_2H_6/C_2H_4 mixture and (e) a 10/90C_2H_6/C_2H_4 mixture and (f) a cycling test of the 50/50C_2H_6/C_2H_4 mixture with a total flow of 1.25 mL min^{-1} in an absorber bed packed with ZJU-120a at 298 K and 1 bar.

efficiently adsorbed by ZJU-120a. During the period between C_2H_4 and C_2H_6 breakthrough, the pure C_2H_4 production of ZJU-120a from the outlet effluent for a given cycle was calculated up to 8.39 L kg^{-1} for 50/50 mixtures. This value is significantly higher than that of most of the top-performing C_2H_6-selective materials reported, such as Cu(Qc)$_2$ (4.3 L kg^{-1})[13] and MAF-49 (6.2 L kg^{-1}).[14] Due to the moderate Q_{st} values of C_2H_6 adsorption, ZJU-120a can be easily regenerated by using a He flow (20 mL min^{-1}) for 15 min at 298 K. Subsequently, we performed multiple mixed-gas (C_2H_6/C_2H_4 at 50/50) column breakthrough tests to investigate the preservation of the separation performance of ZJU-120a under ambient conditions. The recycling experiments showed that the breakthrough performance remains almost unchanged within five continuous cycles (Fig. 3f), confirming its good recyclability for this separation. As inferred from the PXRD experiments on associated samples, ZJU-120a can keep its structure after multiple adsorption tests and breakthrough experiments (Fig. S34, ESI†).

Conclusions

In conclusion, we have demonstrated how a crystal engineering or reticular chemistry approach to pore size control coupled with increasing nonpolar aromatic rings affords porous materials with both exceptional gas uptake capacity and selectivity in the context of C_2H_6/C_2H_4 separation. Two novel ethane-selective MOFs (ZJU-120a and ZJU-121a) were designed and synthesized by altering the carboxylic acid linker in Ni(bdc)(ted)$_{0.5}$, in which the pore size and aromatic rings can be well engineered. The foregoing results indicated that ZJU-120a with the optimized pore size and low-polarity pore surface toward C_2H_6 exhibits simultaneously high C_2H_6 uptake capacity (96 cm^3 g^{-1} at 0.5 bar and 296 K) and excellent C_2H_6/C_2H_4 selectivity (2.74), both of which are much higher than those of Ni(bdc)(ted)$_{0.5}$ and most C_2H_6-selective MOFs developed. In contrast, oversized pores and the absence of nonpolar aromatic rings in Ni(bdc)(ted)$_{0.5}$ or too small pores in ZJU-121a lead to a relatively low C_2H_6 uptake capacity or poor selectivity. Breakthrough experiments confirmed that ZJU-120a can efficiently separate C_2H_6 from C_2H_6/C_2H_4 mixtures to directly produce polymer-grade C_2H_4 with a productivity of 8.39 L kg^{-1}. The design principle revealed in this work is general, which will provide some guidance to facilitate the design and implementation of some new C_2H_6-selective materials with a suitable pore size and nonpolar chemistry for boosting the challenging C_2H_6/C_2H_4 separation.

Experimental section

Synthesis of Ni(ndc)(ted)$_{0.5}$ (ZJU-120)

119 mg (0.5 mmol) nickel(II) chloride hexahydrate ($NiCl_2 \cdot 6H_2O$), 108 mg (0.5 mmol) 1,4-naphthalenedicarboxylic acid (H_2ndc) and 28 mg (0.25 mmol) 1,4-diazabicyclo [2.2.2] octane (ted) were mixed and dissolved in 15 mL DMF. After stirring, the solution was transferred to a Teflon-lined autoclave and heated at 393 K for 2 days. Green crystals of ZJU-120 were obtained by filtering and washed with DMF and methanol.

Synthesis of Ni(adc)(ted)$_{0.5}$ (ZJU-121)

119 mg (0.5 mmol) nickel(II) chloride hexahydrate ($NiCl_2 \cdot 6H_2O$), 133 mg (0.5 mmol) 9,10-anthracenedicarboxylic acid (H_2adc)

and 28 mg (0.25 mmol) 1,4-diazabicyclo [2.2.2] octane (ted) were mixed and dissolved in 15 mL DMF. After stirring, the solution was transferred to a Teflon-lined autoclave and heated at 393 K for 2 days. Dark yellow powder of ZJU-121 was obtained by filtering and washed with DMF and methanol.

Single-crystal X-ray crystallography

Single-crystal X-ray diffraction data of ZJU-120 were collected on a Bruker D8 VENTURE diffractometer at 100 K using graphite-monochromated Mo-Ka (λ = 0.71073 Å) radiation. The structure was solved by a direct method and refined on F2 by full-matrix least-squares methods using SHELXL-97 software package.[27] The solvate molecules of all data were treated as the diffuse contribution to the overall scattering without specific atom positions by using SQUEEZE/PLATON due to the severe disorder of these solvate molecules in the lattices.[28] The crystal data are summarized in Table S1.†

Gas sorption measurements

Adsorption isotherms of C_2H_4 and C_2H_6 were recorded by using a Micromeritics ASAP 2020 surface area analyzer. To remove all the guest solvents in the frameworks, fresh ZJU-120 and ZJU-121 were first solvent-exchanged with dry methanol at least 8 times within two days, wherein 100 mg samples were exchanged with 5 mL methanol each time at room temperature without reflux. The solvent-exchanged samples were evacuated at room temperature for 12 h and then at 423 K for 12 h till the outgas rate was 5 mmHg min^{-1} prior to measurements. The sorption measurement was performed at 77 K with liquid nitrogen. A Julabo water bath is used to keep the adsorption tube at a constant temperature of 273 and 296 K.

Density-functional theory calculations

Our first-principles density functional theory (DFT) calculations were performed using the Quantum-Espresso package.[29] A semiempirical addition of dispersive forces to conventional DFT was included in the calculation to account for van der Waals interactions.[30] We used Vanderbilt-type ultrasoft pseudopotentials and generalized gradient approximation (GGA) with a Perdew–Burke–Ernzerhof (PBE) exchange correlation. A cutoff energy of 544 eV and a 2 × 2 × 2 *k*-point mesh (generated using the Monkhorst–Pack scheme) were found to be enough for the total energy to converge within 0.01 meV per atom. Spin polarization was applied in all calculations, and the two Ni centers in the paddle wheel are coupled antiferromagnetically in the lowest energy state. In both Ni(bdc) $(ted)_{0.5}$ and ZJU-120a structures, the ted ligand and the dicarboxylate ligand are orientationally disordered. To make calculations feasible, we adopted fully ordered structural models, which are approximate representations of the real materials. First, bare MOF structures were fully optimized. For gas adsorption, various possible binding configurations were considered and fully relaxed. The lowest-energy structures were identified as the optimal binding structures. To obtain the gas binding energies, a single gas molecule placed in a supercell with the same cell dimensions was also relaxed as a reference. The static binding energy (at T = 0 K) was calculated using: $E_B = E_{(MOF)} + E_{(gas)} - E_{(MOF+gas)}$. Note that the ligand rotational flexibility/dynamics, which could not be accounted for in our ordered structural models, could also play some role in gas adsorption. Despite this limitation, our calculations still provide helpful qualitative insights into the gas binding mechanisms.

Breakthrough experiments

The breakthrough curves were recorded on a homemade apparatus for gas mixtures C_2H_6/C_2H_4 (50/50) or C_2H_6/C_2H_4 (10/90) at 298 K and 1 bar. In the separation experiment, activated ZJU-120a (0.833 g) particles were prepared and packed into a Φ 4 × 120 mm stainless steel column. The experimental set-up consisted of two fixed-bed stainless steel reactors. One reactor was loaded with the adsorbent, while the other reactor was used as a blank control group to stabilize the gas flow. The gas flows were controlled at the inlet by using a mass flow meter at 1.25 mL min^{-1}, and a gas chromatograph (TCD-Thermal Conductivity Detector, detection limit 0.1 ppm) continuously monitored the effluent gas from the adsorption bed. Prior to every breakthrough experiment, the sample can be generated a He flow (20 mL min^{-1}) for 15 min at 298 K. Subsequently, the column was allowed to equilibrate at the measurement rate before we switched the gas flow.

Conflicts of interest

There are no conflicts to declare.

Acknowledgements

This research was supported by the National Science Foundation of China (51803179), the "National 1000 Young Talent Program", and the "Zhejiang University 100 Talent Program".

Notes and references

1 I. Amghizar, L. A. Vandewalle, K. M. Van Geem and G. B. Marin, *Engineering*, 2017, **3**, 171.
2 T. Ren, M. Patel and K. Blok, *Energy*, 2006, **31**, 425.
3 H. Zimmermann and R. Walzl, *Ullmann's Encyclopedia of Industrial Chemistry*, 2000.
4 R. B. Eldridge, *Ind. Eng. Chem. Res.*, 1993, **32**, 2208.
5 J.-R. Li, R. J. Kuppler and H.-C. Zhou, *Chem. Soc. Rev.*, 2009, **38**, 1477.
6 Y. Wang, S. B. Peh and D. Zhao, *Small*, 2019, **15**, 1900058.
7 R. T. Yang, *Gas Separation by Adsorption Processes*, Butterworth-Heinemann, 2013.
8 (*a*) R. M. Prasad, Y. Iwamoto, R. Riedel and A. Gurlo, *Adv. Eng. Mater.*, 2010, **12**, 522; (*b*) D. A. Pacheco Tanaka, M. A. Llosa Tanco, J. Okazaki, Y. Wakui, F. Mizukami and T. M. Suzuki, *J. Membr. Sci.*, 2008, **320**, 436; (*c*) P. J. Bereciartua, Á. Cantín, A. Corma, J. L. Jordá, M. Palomino, F. Rey, S. Valencia, E. W. Corcoran, P. Kortunov, P. I. Ravikovitch, A. Burton, C. Yoon, Y. Wang,

C. Paur, J. Guzman, A. R. Bishop and G. L. Casty, *Science*, 2017, **358**, 1068.

9 (*a*) H. Furukawa, K. E. Cordova, M. O'Keeffe and O. M. Yaghi, *Science*, 2013, **341**, 6149; (*b*) Y. He, R. Krishna and B. Chen, *Energy Environ. Sci.*, 2012, **5**, 9107; (*c*) K. Adil, Y. Belmabkhout, R. S. Pillai, A. Cadiau, P. M. Bhatt, A. H. Assen, G. Maurin and M. Eddaoudi, *Chem. Soc. Rev.*, 2017, **46**, 3402; (*d*) X. Zhao, Y. Wang, D.-S. Li, X. Bu and P. Feng, *Adv. Mater.*, 2018, **30**, 1705189; (*e*) B. Li, H.-M. Wen, Y. Yu, Y. Cui, W. Zhou, B. Chen and G. Qian, *Mater. Today*, 2018, **2**, 21; (*f*) M. Ding, R. W. Flaig, H.-L. Jiang and O. M. Yaghi, *Chem. Soc. Rev.*, 2019, **48**, 2783.

10 (*a*) E. D. Bloch, W. L. Queen, R. Krishna, J. M. Zadrozny, C. M. Brown and J. R. Long, *Science*, 2012, **335**, 1606; (*b*) S. Yang, A. J. Ramirez-Cuesta, R. Newby, V. Garcia-Sakai, P. Manuel, S. K. Callear, S. I. Campbell, C. C. Tang and M. Schröder, *Nat. Chem.*, 2015, **7**, 121; (*c*) J. E. Bachman, M. T. Kapelewski, D. A. Reed, M. I. Gonzalez and J. R. Long, *J. Am. Chem. Soc.*, 2017, **139**, 15363; (*d*) Z. Bao, J. Wang, Z. Zhang, H. Xing, Q. Yang, Y. Yang, H. Wu, R. Krishna, W. Zhou, B. Chen and Q. Ren, *Angew. Chem., Int. Ed.*, 2018, **130**, 16252; (*e*) R.-B. Lin, L. Li, H.-L. Zhou, H. Wu, C. He, S. Li, R. Krishna, J. Li, W. Zhou and B. Chen, *Nat. Mater.*, 2018, **17**, 1128; (*f*) B. Li, Y. Zhang, R. Krishna, K. Yao, Y. Han, Z. Wu, D. Ma, Z. Shi, T. Pham, B. Space, J. Liu, P. K. Thallapally, J. Liu, M. Chrzanowski and S. Ma, *J. Am. Chem. Soc.*, 2014, **136**, 8654.

11 (*a*) A. Cadiau, K. Adil, P. Bhatt, Y. Belmabkhout and M. Eddaoudi, *Science*, 2016, **353**, 137; (*b*) Y.-S. Bae, C. Y. Lee, K. C. Kim, O. K. Farha, P. Nickias, J. T. Hupp, S. T. Nguyen and R. Q. Snurr, *Angew. Chem., Int. Ed.*, 2012, **51**, 1857; (*c*) K. Li, D. H. Olson, J. Seidel, T. J. Emge, H. Gong, H. Zeng and J. Li, *J. Am. Chem. Soc.*, 2009, **131**, 10368; (*d*) H. Wang, X. Dong, V. Colombo, Q. Wang, Y. Liu, W. Liu, X. L. Wang, X. Y. Huang, D. M. Proserpio, A. Sironi, Y. Han and J. Li, *Adv. Mater.*, 2018, **30**, 1805088.

12 L. Li, R.-B. Lin, R. Krishna, H. Li, S. Xiang, H. Wu, J. Li, W. Zhou and B. Chen, *Science*, 2018, **362**, 443.

13 R.-B. Lin, H. Wu, L. Li, X.-L. Tang, Z. Li, J. Gao, H. Cui, W. Zhou and B. Chen, *J. Am. Chem. Soc.*, 2018, **140**, 12940.

14 P.-Q. Liao, W.-X. Zhang, J.-P. Zhang and X.-M. Chen, *Nat. Commun.*, 2015, **6**, 8697.

15 W. Liang, F. Xu, X. Zhou, J. Xiao, Q. Xia, Y. Li and Z. Li, *Chem. Eng. Sci.*, 2016, **148**, 275.

16 X. Wang, Z. Niu, A. M. Al-Enizi, A. Nafady, Y. Wu, B. Aguila, G. Verma, L. Wojtas, Y.-S. Chen, Z. Li and S. Ma, *J. Mater. Chem. A*, 2019, **7**, 13585.

17 O. T. Qazvini, R. Babarao, Z.-L. Shi, Y.-B. Zhang and S. G. Telfer, *J. Am. Chem. Soc.*, 2019, **141**, 5014.

18 Y. Chen, Z. Qiao, H. Wu, D. Lv, R. Shi, Q. Xia, J. Zhou and Z. Li, *Chem. Eng. Sci.*, 2018, **175**, 110.

19 (*a*) H. G. Hao, Y. F. Zhao, D. M. Chen, J. M. Yu, K. Tan, S. Ma, Y. Chabal, Z. M. Zhang, J. M. Dou, Z. H. Xiao, G. Day, H. C. Zhou and T. B. Lu, *Angew. Chem., Int. Ed.*, 2018, **130**, 16299; (*b*) J. Pires, M. L. Pinto and V. K. Saini, *ACS Appl. Mater. Interfaces*, 2014, **6**, 12093; (*c*) M. Hartmann, U. Böhme, M. Hovestadt and C. Paula, *Langmuir*, 2015, **31**, 12382; (*d*) J. Pires, J. Fernandes, K. Dedecker, J. R. Gomes, G. Perez-Sanchez, F. Nouar, C. Serre and M. L. Pinto, *ACS Appl. Mater. Interfaces*, 2019, **11**, 27410; (*e*) H. Zeng, X.-J. Xie, M. Xie, Y.-L. Huang, D. Luo, T. Wang, Y. Zhao, W. Lu and D. Li, *J. Am. Chem. Soc.*, 2019, **141**, 20390.

20 (*a*) R. P. Ribeiro, B. C. Camacho, A. Lyubchyk, I. A. Esteves, F. J. Cruz and J. P. Mota, *Microporous Mesoporous Mater.*, 2016, **230**, 154; (*b*) R. S. Pillai, M. L. Pinto, J. Pires, M. Jorge and J. R. Gomes, *ACS Appl. Mater. Interfaces*, 2015, **7**, 624; (*c*) C. Gücüyener, J. van den Bergh, J. Gascon and F. Kapteijn, *J. Am. Chem. Soc.*, 2010, **132**, 17704; (*d*) U. Böhme, B. Barth, C. Paula, A. Kuhnt, W. Schwieger, A. Mundstock, J. Caro and M. Hartmann, *Langmuir*, 2013, **29**, 8592.

21 (*a*) H. Zeng, M. Xie, Y.-L. Huang, Y. Zhao, X.-J. Xie, J.-P. Bai, M.-Y. Wan, R. Krishna, W. Lu and D. Li, *Angew. Chem., Int. Ed.*, 2019, **58**, 8515; (*b*) L. Li, H.-M. Wen, C. He, R.-B. Lin, R. Krishna, H. Wu, W. Zhou, J. Li, B. Li and B. Chen, *Angew. Chem., Int. Ed.*, 2018, **57**, 15183; (*c*) X. Cui, K. Chen, H. Xing, Q. Yang, R. Krishna, Z. Bao, H. Wu, W. Zhou, X. Dong, Y. Han, B. Li, Q. Ren, M. J. Zaworotko and B. Chen, *Science*, 2016, **353**, 141; (*d*) P. Nugent, Y. Belmabkhout, S. D. Burd, A. J. Cairns, R. Luebke, K. Forrest, T. Pham, S. Ma, B. Space, L. Wojtas, M. Eddaoudi and M. J. Zaworotko, *Nature*, 2013, **495**, 80; (*e*) T. Kundu, B. B. Shah, L. Bolinois and D. Zhao, *Chem. Mater.*, 2019, **31**, 2842.

22 (*a*) K.-J. Chen, D. G. Madden, S. Mukherjee, T. Pham, K. A. Forrest, A. Kumar, B. Space, J. Kong, Q.-Y. Zhang and M. J. Zaworotko, *Science*, 2019, **366**, 241; (*b*) Y.-P. Li, Y. Wang, Y.-Y. Xue, H.-P. Li, Q.-G. Zhai, S.-N. Li, Y.-C. Jiang, M.-C. Hu and X. Bu, *Angew. Chem., Int. Ed.*, 2019, **58**, 13590; (*c*) W. Fan, X. Wang, X. Zhang, X. Liu, Y. Wang, Z. Kang, F. Dai, B. Xu, R. Wang and D. Sun, *ACS Cent. Sci.*, 2019, **5**, 1261; (*d*) S.-J. Bao, R. Krishna, Y.-B. He, J.-S. Qin, Z.-M. Su, S.-L. Li, W. Xie, D.-Y. Du, W.-W. He, S.-R. Zhang and Y.-Q. Lan, *J. Mater. Chem. A*, 2015, **3**, 7361; (*e*) H.-R. Fu and J. Zhang, *Chem.–Eur. J.*, 2015, **21**, 5700; (*f*) B. Li, X. Cui, D. O'Nolan, H.-M. Wen, M. Jiang, R. Krishna, H. Wu, R.-B. Lin, Y.-S. Chen, D. Yuan, H. Xing, W. Zhou, Q. Ren, G. Qian, M. J. Zaworotko and B. Chen, *Adv. Mater.*, 2017, **29**, 1704210.

23 (*a*) L. Liang, C. Liu, F. Jiang, Q. Chen, L. Zhang, H. Xue, H.-L. Jiang, J. Qian, D. Yuan and M. Hong, *Nat. Commun.*, 2017, **8**, 1233; (*b*) L. Li, X. Wang, J. Liang, Y. Huang, H. Li, Z. Lin and R. Cao, *ACS Appl. Mater. Interfaces*, 2016, **8**, 9777; (*c*) C. Gu, N. Hosono, J.-J. Zheng, Y. Sato, S. Kusaka, S. Sakaki and S. Kitagawa, *Science*, 2019, **363**, 387; (*d*) P. Li, N. A. Vermeulen, C. D. Malliakas, D. A. Gómez- Gualdrón, A. J. Howarth, B. L. Mehdi, A. Dohnalkova, N. D. Browning, M. O'Keeffe and O. K. Farha, *Science*, 2017, **356**, 624; (*e*) X. Song, M. Zhang, C. Chen, J. Duan, W. Zhang, Y. Pan and J. Bai, *J. Am. Chem. Soc.*, 2019, **141**, 14539.

24 (*a*) H. He, F. Sun, B. Aguila, J. A. Perman, S. Ma and G. Zhu, *J. Mater. Chem. A*, 2016, **4**, 15240; (*b*) H.-M. Wen, C. Liao, L. Li, H. Wu, W. Zhou, J. Hu and B. Chen, *J. Mater. Chem. A*, 2019, **7**, 3128; (*c*) H. Wang, X. Dong, J. Lin, S. J. Teat, S. Jensen,

J. Cure, E. V. Alexandrov, Q. Xia, K. Tan, Q. Wang, D. H. Olson, D. M. Proserpio, Y. J. Chabal, T. Thonhauser, J. Sun, Y. Han and J. Li, *Nat. Commun.*, 2018, **9**, 1745; (*d*) L. Li, R.-B. Lin, R. Krishna, X. Wang, B. Li, H. Wu, J. Li, W. Zhou and B. Chen, *J. Am. Chem. Soc.*, 2017, **139**, 7733; (*e*) H.-M. Wen, B. Li, L. Li, R.-B. Lin, W. Zhou, G. Qian and B. Chen, *Adv. Mater.*, 2018, **30**, 1704792.

25 (*a*) P.-Q. Liao, N.-Y. Huang, W.-X. Zhang, J.-P. Zhang and X.-M. Chen, *Science*, 2017, **356**, 1193; (*b*) Y. Ye, Z. Ma, R.-B. Lin, R. Krishna, W. Zhou, Q. Lin, Z. Zhang, S. Xiang and B. Chen, *J. Am. Chem. Soc.*, 2019, **141**, 4130; (*c*) X. Zhao, J. G. Bell, S.-F. Tang, L. Li and K. M. Thomas, *J. Mater. Chem. A*, 2016, **4**, 1353; (*d*) Z. R. Herm, B. M. Wiers, J. A. Mason, J. M. van Baten, M. R. Hudson, P. Zajdel, C. M. Brown, N. Masciocchi, R. Krishna and J. R. Long, *Science*, 2013, **340**, 960; (*e*) Y.-L. Peng, T. Pham, P. Li, T. Wang, Y. Chen, K.-J. Chen, K. A. Forrest, B. Space, P. Cheng, M. J. Zaworotko and Z. Zhang, *Angew. Chem., Int. Ed.*, 2018, **57**, 10971.

26 (*a*) G. Xu, B. Li, H. Wu, W. Zhou and B. Chen, *Cryst. Growth Des.*, 2017, **17**, 4795; (*b*) H.-M. Wen, L. Li, R.-B. Lin, B. Li, B. Hu, W. Zhou, J. Hu and B. Chen, *J. Mater. Chem. A*, 2018, **6**, 6931.

27 (*a*) A. Altomare, G. Cascarano, C. Giacovazzo and A. Guagliardi, *J. Appl. Crystallogr.*, 1994, **27**, 435; (*b*) G. M. Sheldrick, *Acta Crystallogr., Sect. A: Found. Crystallogr.*, 2008, **64**, 112.

28 A. L. Spek, *J. Appl. Crystallogr.*, 2003, **36**, 7.

29 P. Giannozzi, S. Baroni, N. Bonini, M. Calandra, R. Car, C. Cavazzoni, D. Ceresoli, G. L. Chiarotti, M. Cococcioni, I. Dabo, A. Dal Corso, S. Fabris, G. Fratesi, S. de Gironcoli, R. Gebauer, U. Gerstmann, C. Gougoussis, A. Kokalj, M. Lazzeri, L. Martin-Samos, N. Marzari, F. Mauri, R. Mazzarello, S. Paolini, A. Pasquarello, L. Paulatto, C. Sbraccia, S. Scandolo, G. Sclauzero, A. P. Seitsonen, A. Smogunov, P. Umari and R. M. Wentzcovitch, *J. Phys.: Condens. Matter*, 2009, **21**, 395502.

30 V. Barone, M. Casarin, D. Forrer, M. Pavone, M. Sambi and A. Vittadini, *J. Comput. Chem.*, 2009, **30**, 934.

